Hubble Space Telescope Observations of M31 associations

Magnier, E.A.; Hodge, P.; Battinelli, P.; Lewin, W.H.G.; van Paradijs, J.A.

DOI
10.1093/mnras/292.3.490
Publication date
1997

Published in
Monthly Notices of the Royal Astronomical Society

Mon. Not. R. Astron. Soc. **292,** 490–498 (1997)

Hubble Space Telescope observations of M31 associations

Eugene A. Magnier,[1⋆] Paul Hodge,[1⋆] Paolo Battinelli,[2⋆] Walter H. G. Lewin[3⋆] and Jan van Paradijs[4,5⋆]

[1] *University of Washington, Astronomy Department 351580, Seattle, WA 98195-1580, USA*
[2] *Osservatorio Astronomico di Roma, Viale del Parco Mellini 84, I-00136 Roma, Italy*
[3] *Massachusetts Institute of Technology, 37-624, Cambridge, MA 02139, USA*
[4] *Astronomical Institute 'Anton Pannekoek' and Center for High Energy Astrophysics, University of Amsterdam, Kruislaan 403, 1098 SJ Amsterdam, the Netherlands*
[5] *Physics Department, University of Alabama in Huntsville, Huntsville, AL 35899, USA*

Accepted 1997 July 1. Received 1997 June 24; in original form 1997 April 21

ABSTRACT

We have used *HST* WFPC-2 observations of five fields along the eastern spiral arm regions of M31 to study the stellar populations. We use fits to stellar models to determine extinction individually for the stars in OB associations in these fields. The range of extinction within each cluster is the major constraint on our ability to determine accurate parameters for each association. We are able to determine ages of the clusters to ~0.2 in log age, which is sufficient to distinguish between the older and younger associations. These observations provide us with the first measurement of the ages of young star clouds in M31 and allow us to make comparisons with other, less well-calibrated tracers of the association ages, in particular the Hα and H I morphologies.

Key words: stars: early-type – stars: formation – galaxies: individual: M31 – galaxies: spiral – galaxies: star clusters – galaxies: stellar content.

1 INTRODUCTION

M31 is a popular place in which to attempt studies of stellar populations, particularly the young, massive stellar component. It has many potential advantages for such studies over the Galaxy. By virtue of the fact that we observe it from outside, the extinction is low compared with much of the Galactic disc, and it is easy to determine the positions of the stars relative to features of the disc, such as the H I or other tracers of the spiral arms. Furthermore, the distance is well determined, and all M31 stars can be considered to be at that same distance (~700 kpc). Unlike the Magellanic Clouds, M31 is a spiral galaxy, and therefore is more easily comparable with the Milky Way.

Many groups have studied the young stellar population of M31, starting with Hubble (1929). Baade (1944) identified the Population I/ Population II dichotomy in large part on the basis of observations of M31. More recently, several groups have attempted to use wide-band photometry of portions of M31 to study the properties of the populations. There have been several studies of a few OB associations using ground-based CCD photometry, usually with some subset of *UBVRI* filters (see e.g. Richer & Crabtree 1985; Massey, Armandroff & Conti 1986; Hodge & Lee 1988; Hodge, Lee & Mateo 1988; Freedman 1989). A more complete CCD survey of the entire M31 disc was performed by Magnier et al. (1992) and Haiman et al. (1994a). These observations have been used for several studies, including studies of the properties of associations on the basis of colour–magnitude diagrams (CMDs) (Haiman et al. 1994b).

These studies have shown some of the difficulties of using ground-based observations of M31 OB associations to study the recent star formation. Perhaps the single most important problem for these ground-based studies is the effect of crowding. In these studies, the observed CMDs show a 'blue spur' corresponding to the upper end of the main sequence. This blue spur is quite broad from the combined effects of crowding, variable extinction, and age ranges. It has been difficult to disentangle these various effects, making it extremely difficult to determine ages, or even relative ages, of the associations. More subtle details, such as the slope of the initial mass function (IMF) of these associations, are definitely beyond the scope of these ground-based data. Judging from recent results in the Large Magellanic Cloud (LMC) in which CCD photometry in crowded fields has resulted in highly improved CMDs, we concluded that the crowding was the single largest problem for M31 associations. In this study, we have used the *Hubble Space Telescope* (*HST*) to circumvent the severe problems of crowding.

2 OBSERVATIONS AND ANALYSIS

We have observed five fields in M31 with *HST*. The fields were chosen along the eastern spiral arm regions where there are many

⋆E-mail: gene@astro.washington.edu (EAM); hodge@astro.washington.edu (PH); battinel@oarhp1.rm.astro.it (PB); lewin@space.mit.edu (WHGL); jvp@astro.uva.nl (JvP)

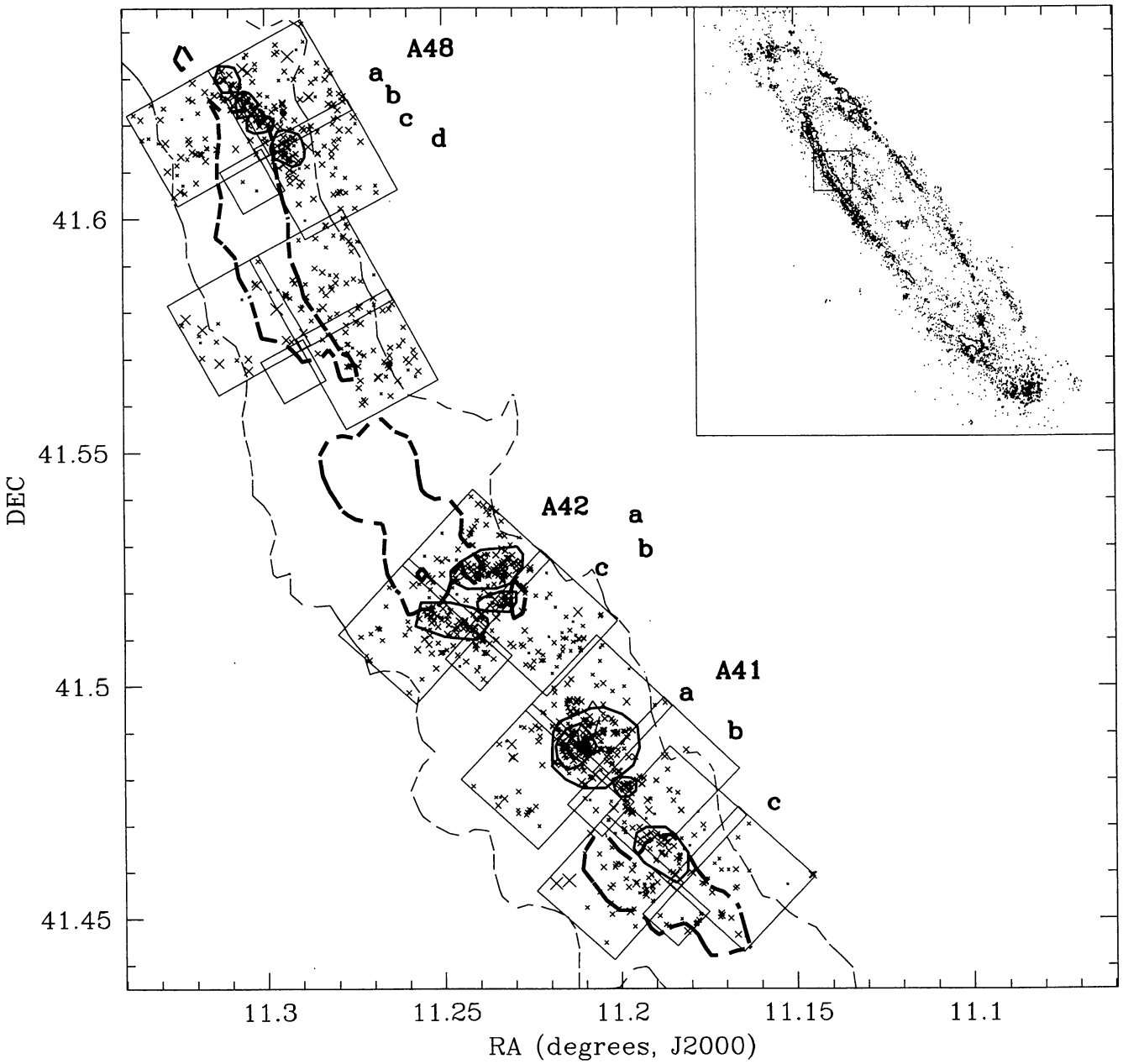

Figure 1. A map of our *HST* observations in M31. The ×s mark the locations of stars with $V < 22$, with the size scaled by colour (larger crosses are bluer). The thick and thin dashed lines are H I contours from the H I map of Brinks & Shane (1984), and the heavy solid contours show the location of Efremov, Ivanov & Nikolov's (1987) OB associations. The inset shows the location of these observations in the full disc of M31, with both H I contours and blue stars from the MIT/Amsterdam survey (Magnier et al. 1992; Haiman et al. 1994a).

sites of recent star formation (Fig. 1). The five fields are grouped into two contiguous regions, with three in the southern region and two in the northern region. For each field, Wide Field Planetary Camera 2 (WFPC-2) images were taken with four filters, F555W (roughly V), F439W (roughly B), F330W (roughly U) and F160BW. Two images were taken for each of the F160BW and F330W filters with exposure times of 500 and 60 s, and 400 and 40 s, respectively. Only single F555W and F439W filter images were taken of each field with exposure times of 140 and 160 s. In this analysis, we have used only the V, B and long U images as the F160BW filters were found to have significantly lower throughput than expected (see also Bertola et al. 1995).

The first important step in reducing WFPC-2 images is to clean the images of cosmic rays. A serious difficulty with the WFPC-2 CCDs is the undersampling of the point spread function (PSF), which makes it very difficult to distinguish cosmic rays and real stars. A standard solution to this problem is to take at least two exposures of similar duration per filter, and use a program such as the IRAF CRREJ routine. This routine rejects cosmic rays by checking for pixels that are significantly different between the two frames. In our case, however, we do not have the data to use such a technique since we have only a single image per field for most filters. In our analysis, we have identified cosmic rays by finding those objects in which the U, B and V colours are highly anomalous. In particular,

since the U images are by far the longest, most cosmic rays show up as 'stars' with impossibly blue $U-V$ and $U-B$ colours.

The next step in the analysis is to obtain photometry from the images. First, we applied the geometric correction image (see Holtzman et al. 1995) to the three WFPC images. This image removes a correction applied to account for the geometric distortion in the WFPC optical system. The distortion makes the effective areas of pixels near the edges of the CCDs larger than near the centre, altering the photometry of extended objects. The correction applied by STScI corrects the photometry for extended objects, but makes the photometry incorrect for point sources. The image that we applied removes this correction. Next, we used the PSF fitting routine DOPHOT to determine the fluxes for all stars. This program uses an analytical representation of the PSF to determine the stellar fluxes. After DOPHOT was run on the images, a series of corrections was applied to convert the instrumental magnitudes to appropriate *HST* magnitudes. The conversions, detailed in Holtzman et al. (1995), are as follows. First, we applied a correction to account for the differently sized aperture boxes used by Holtzman et al. (1995) and our DOPHOT run, as well as the difference between the analytical fit in DOPHOT and the flux in a fixed aperture. Secondly, we applied a correction dependent on the row number position of each star to account for the CTE effect described by Holtzman et al. (1995). Finally, we applied the zero-point values given by Holtzman et al. (1995). We used the zero-points that are appropriate for the magnitude system based on the observed flux of Vega (see Holtzman et al. 1995; Whitmore 1995). A comparison between our overlapping fields (on different WFPC chips) shows that our photometric accuracy is ~0.03 mag, with no evidence of systematic trends in colour or magnitude. There is a tendency for the brighter stars to compare less well, with the brightest stars ($\lesssim$18 mag) having errors of ~0.05 mag.

3 ASSOCIATION CMDs

Fig. 1 shows a map of our two regions with the observed stars overlaid with H I contours from Brinks & Shane (1984). The point size is related to the colour of the star, with the largest points having $U-V<-2.0$ and the smallest points having $U-V>0.0$. Such a scaling allows a qualitative determination of the regions with the youngest stars. Stars with $V>22$ are not plotted. As expected, most of the blue, young stars are arranged in rough groups. The OB association boundaries determined by Efremov et al. (1987) are shown. These boundaries appear to represent the important large groupings, but smaller groupings, both internal and external to these associations, can be seen. Throughout the rest of this paper, we will concentrate on the properties of these OB associations, in comparison with each other and with the 'field' stars. However, it is important for the reader to realize that the definitions of these associations are somewhat arbitrary, and should be considered as representative rather than definitive (see e.g. the discussion by Battinelli, Efremov & Magnier 1996). In Fig. 1, the associations are labelled with the names designated by Efremov et al. (1987), based on the original designations of van den Bergh (1964).

Fig. 2 shows colour–magnitude and colour–colour diagrams for one of the richest associations in the data set. This is the association labelled A42a in Fig. 1. We will discuss some of the aspects of these diagrams as an example for the rest of the associations. Included in this CMD are solar metallicity isochrones from Bertelli et al. (1994). These isochrones are given in terms of Johnson *UBV* magnitudes, so we have corrected the isochrones to the WFPC-2 system using the corrections described by Holtzman et al. (1995). Bertelli et al. (1994) present isochrones with logarithmic ages in the range 6.6 to 10.3 log(yr) with spacing of 0.1 log(yr). We plot only a few representative isochrones here. For this field, we have incorporated an extinction of $A_V=1.1$ mag for plotting the isochrones, as discussed below.

We first note that this CMD is greatly improved over ground-based CMDs produced in the past: there is a narrow 'blue plume' corresponding to the upper end of the main sequence and evolved massive stars. As a comparison, the width of the blue plume in the $V, B-V$ diagram is ~0.2 mag at $V=20$ in our observations and >0.7 the paper by Hodge & Lee (1988) or Haiman et al. (1994b). This improvement is almost certainly due to the near-elimination of the severe crowding problems in the ground-based data.

The next important point to note is that there is significant extinction and range of extinction for this association, and indeed for all of the associations in our observations. This can most easily be seen in the *UBV* colour–colour diagram (Fig. 2, right-hand panel). In this diagram, we have plotted the unextinguished isochrones, as well as the reddening line. This reddening line is calculated using the central wavelengths of the WFPC-2 filters applied to the parametrized extinction law of Cardelli, Clayton & Mathis (1989), using $R_V=3.1$. From this diagram, it can be seen

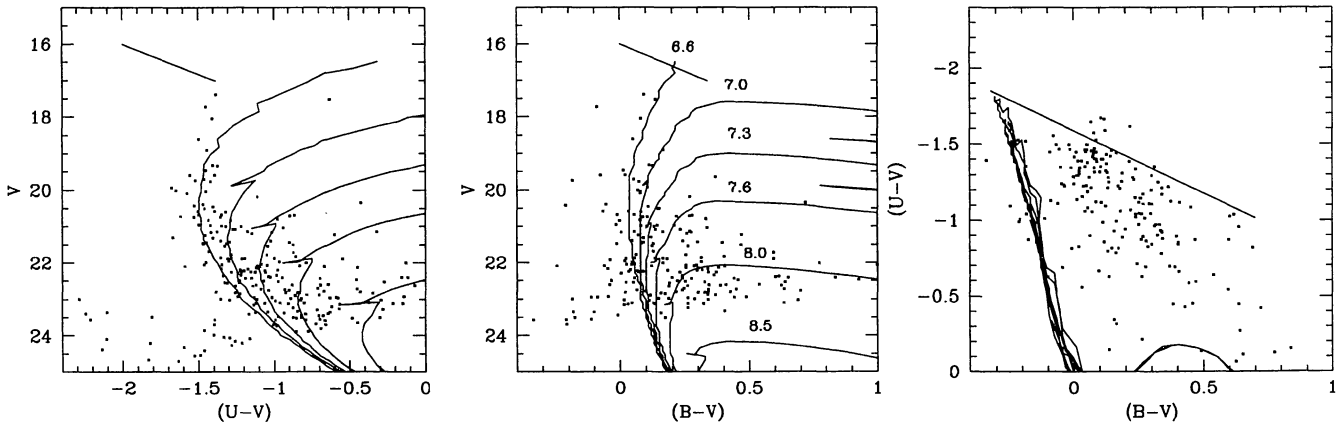

Figure 2. OB association A42a. The left-hand and middle panels show CMDs in $V, U-V$ and $V, B-V$ respectively, corrected for $A_V=1.2$ mag. Both include isochrones from Bertelli et al. (1994) with log(ages) of 6.6, 7.0, 7.3, 7.6, 8.0 and 8.5 yr. The diagonal line shows the effect of extinction ($A_V=1$). The right-hand panel shows a $B-V, U-V$ colour–colour diagram, with the same isochrones and a line showing the effect of extinction.

that a single extinction does not appear to be sufficient to correct all the stars. A range of extinction from $A_V \sim 0.4$ to 1.5 appears to be reasonable for this field. The apparent range of extinction in this field cannot be explained simply by photometric errors, as the required errors would have to be in the vicinity of 0.2 mag, almost a factor of 10 larger than our errors. Furthermore, there are clear groupings of stars with different levels of extinction which would be difficult to produce with random errors. A large range of extinction appears to be typical in the associations in our observations, as expected if much of the original molecular clouds have not yet been dispersed, and as is seen in Galactic associations. As we discuss below, this single aspect introduces the bulk of the error in our determination of the association properties.

3.1 Extinction determination

In order to draw conclusions from the CMD, it is necessary to correct for the effects of extinction. An average correction is probably not sufficient since most of these associations show a large range of extinction: an average correction would introduce errors of roughly 0.5 mag in V in most cases. One possible method to correct for the extinction is to use the colour–colour diagram and 'slide' each star back to the locus of unextinguished stars. There are several drawbacks to this process. First, it is difficult to incorporate the photometric errors in this method. By forcing the stars to lie on the locus of unextinguished stars, the method effectively amplifies the effects of errors in the three photometric bands. This is particularly a problem because of the small angle between the reddening line and the locus of stars: if all three bands (*UBV*) have roughly equal errors, the error in A_V will be roughly 5 times as large as the photometric error in a single band. For this same reason, it is unclear what to do with any stars that lie above the reddening line from the bluest stars ($U - V < -1.72$). Such a colour must be due to photometric errors, but there is no clear best value for their true unreddened colours. Finally, this method makes no use of the luminosity information, so that stars may be given extinction values that lead to unrealistic luminosities, particularly those stars that are consistent with positions at the bluest end of the locus.

To minimize the introduction of errors in determining the extinction for individual stars, we have made use of the luminosity and colour information to determine approximate extinction values for the stars. For every star, we assign a distance modulus of 24.25 (700 kpc: Welch et al. 1986) and allow the extinction (A_V) to take on values of 0.0 to 3.1 in steps of 0.1 mag. We then calculate the expected absolute magnitudes for each star and compare these with the absolute magnitudes for every star in the Bertelli et al. (1994) isochrones, determining the χ^2 for the star, extinction and model. In general, a particular star may be well fitted by a large number of models, especially those that have colours similar to the main sequence, where the density of model stars in the colour–colour plane is quite high. We calculate an average value for the extinction from the five best-fitting models, incorporating a weighting factor

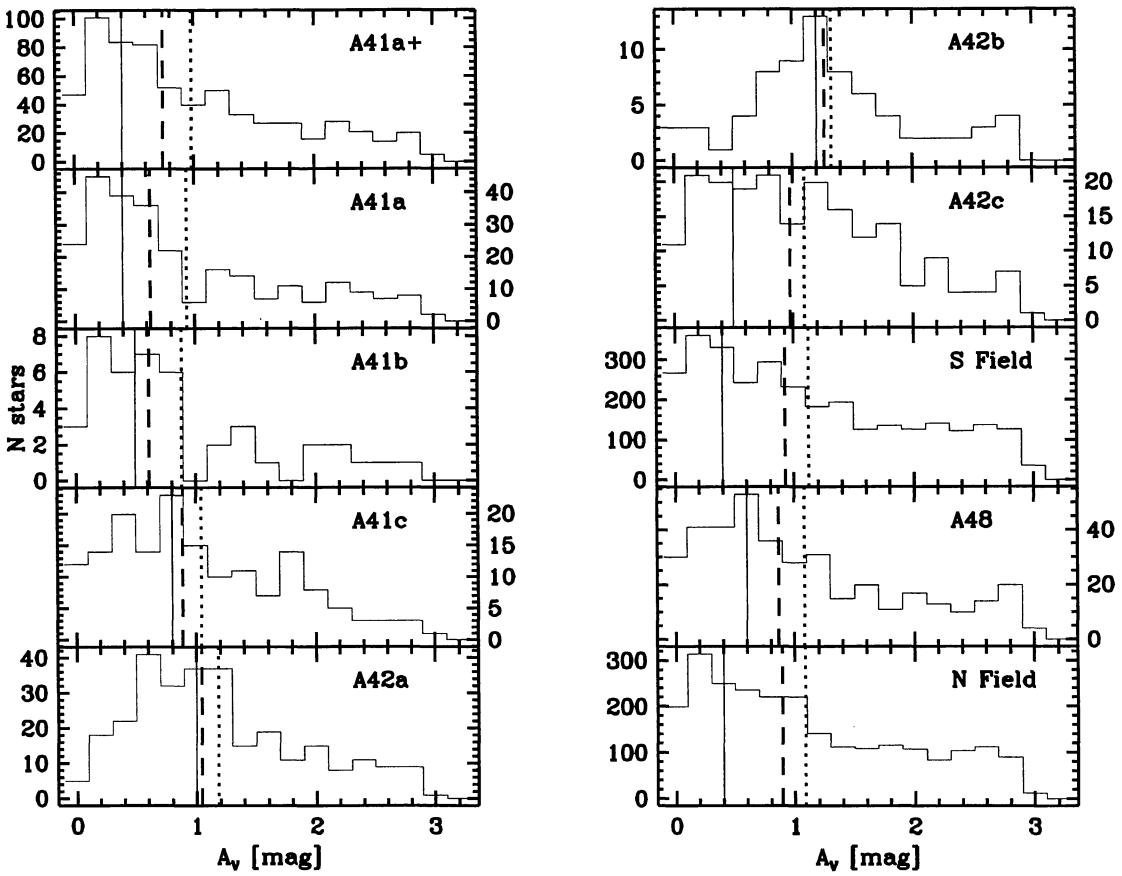

Figure 3. Extinction distributions for each association. We plot the measured extinctions for the stars of each association, and all non-association stars for the northern and southern fields. In each figure, the solid line shows the adopted value used in the corrected CMDs (below), the dashed line shows the median value and the dotted line shows the mean value.

dependent on the χ^2, to let the better models have a somewhat higher impact on the average.

We have used a set of Monte Carlo simulations to compare this method of determining the extinction with the colour–colour diagram method. For each Bertelli et al. (1994) isochrone, we generated fake stars with 10 per cent Gaussian photometric errors and 1 mag of extinction (A_V). We then applied both methods of dereddening and compared the recovered CMD with the original isochrone. The result is quite encouraging. The recovered A_V values using the colour–colour diagram method have a typical scatter of 0.54–0.65 mag, while those recovered using the isochrone fitting have a scatter in the range 0.38–0.44. Even so, it is clear that the dereddening process introduces a significant amount of error. If it were possible to assume a single average extinction for a given association, we would be more easily able to interpret the CMDs. However, as seen above, it is unlikely that a single extinction is valid for any particular association.

For each of the associations shown in Fig. 1, we have determined the distribution of extinction using the isochrone fitting method. Fig. 3 shows histograms of A_V for each of the seven associations and the surrounding field stars. It is possible to distinguish variations in the average extinction between associations. For example, association A41a has a significantly lower extinction than A42a. A41a, for example, has a mean extinction consistent with only foreground extinction ($A_V \approx 0.25$ – Humphreys 1979; Burstein & Heiles 1984). The range of extinction seen for A41a (± 0.2 mag) is probably indicative of our ability to determine the extinction for a given association. It is also clear that some associations have a small range of extinctions (like A41a), while others appear to have a wide range (e.g. A41c), or even a few discrete values for the extinction (e.g. A41b). This latter effect may be the result of distinct small-scale groupings within the association, or the clumpiness of the interstellar clouds.

It is useful to compare the distribution of the stellar extinction with related tracers, in particular the location of H I emission. For both the northern and southern regions, we have defined a grid on the sky with boxes roughly 20 arcsec on a side. For each box, we have determined the average extinction value for all stars within the box. There is only a weak correlation between the H I column density and the measured extinction. Fig. 4 shows a plot of the extinction versus the H I column density. The solid line labelled $N_H \rightarrow A_V$ shows the expected relationship if the stars are behind the H I and the gas-to-dust ratio is the same in M31 as in the Galaxy (Zombeck 1990). A second solid line labelled $N_H \rightarrow 2A_V$ shows the expected relationship if the stars lie on average at the centre of the gas, so that the dust associated with only half of the observed H I contributes to the extinction. Clearly, there is too little extinction for either of these descriptions. The relationship is better represented by the line in which the average extinction comes from the dust associated with only one-third of the average N_H. There are several possible ways to explain this situation. It might be that the gas-to-dust ratio in M31 is significantly different from the average Galactic value used as a comparison here. Comparisons between *IRAS* observations of the emission from dust and H I maps of M31 show a possible radial variation in the gas-to-atomic hydrogen ratio, with uncertainties in the vicinity of 50 per cent (Walterbos & Schwering 1987), so this remains a possibility. Alternatively, this may show that the typical location of the observed stars is only one-third of the way into the H I arm. This is also possible: what appears to be a single spiral arm in this region is probably in fact two arms projected on the same line of sight. The H I emission seen along this portion of M31 is split into two velocity

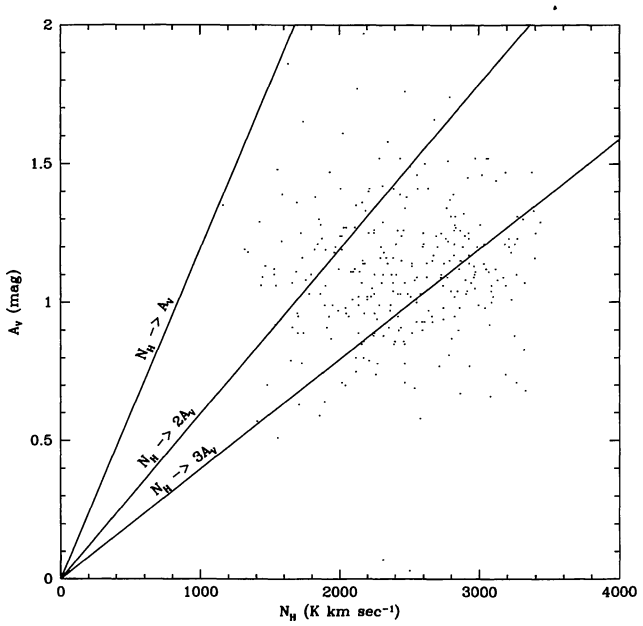

Figure 4. Comparison of the average A_V and the H I column density. The three lines show the expected relationship if the extinction is caused by all of the H I, one-half or one-third of the H I.

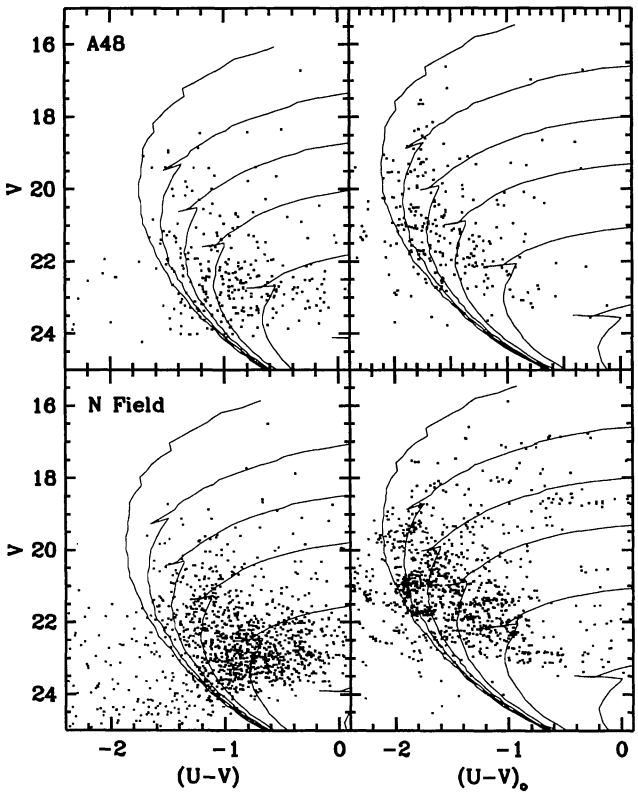

Figure 5. CMDs for associations in the northern fields. Each figure contains isochrones from Bertelli et al. (1994; see Fig. 2). The left-hand plots of each pair have been corrected for a single, typical extinction (see Fig. 3); the right-hand plots have been corrected on a star-by-star basis.

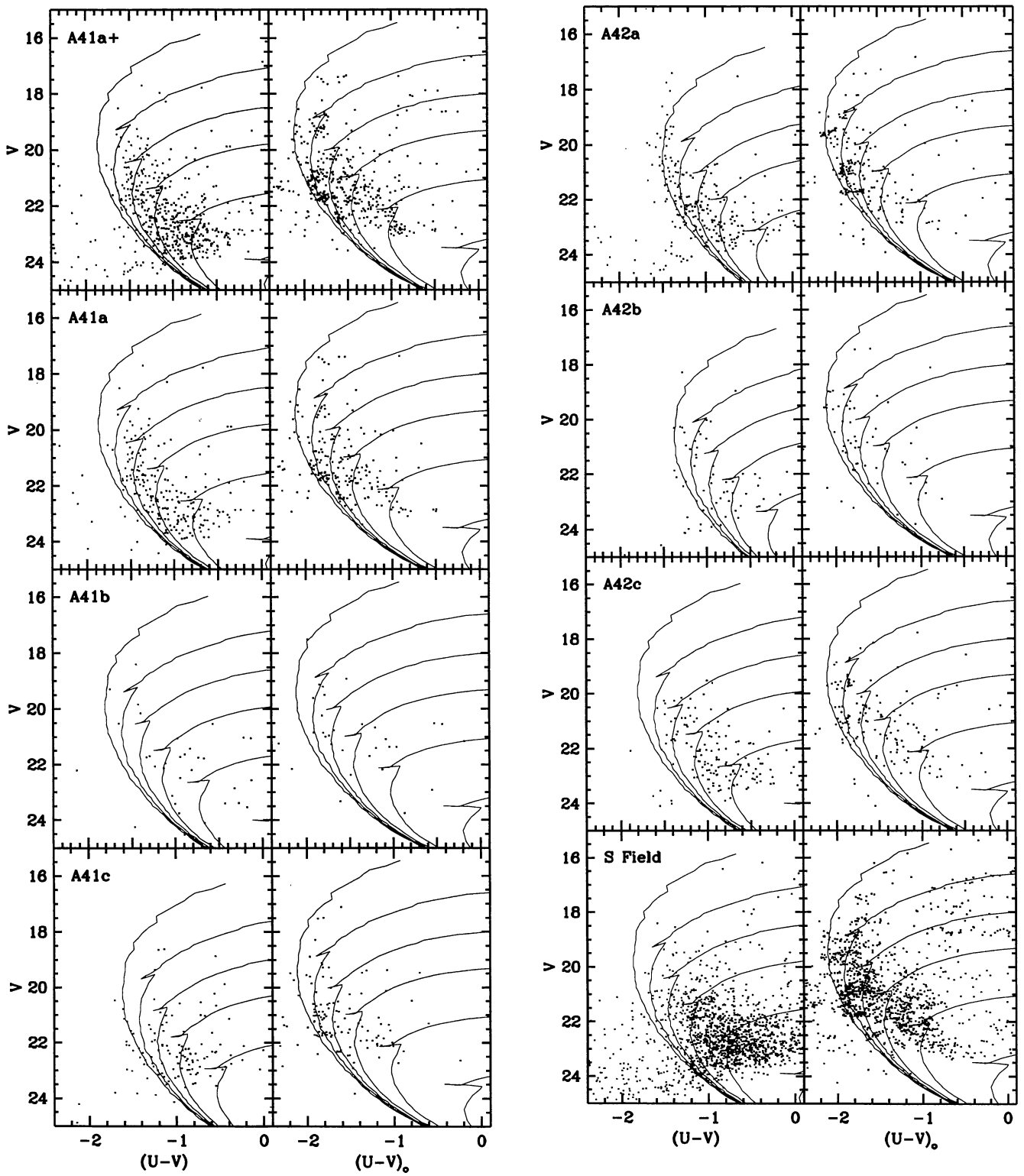

Figure 6. CMDs for associations in the southern fields. A41a+ is the larger region surrounding A41a. See Fig. 5.

components due to the warp in the M31 disc (Brinks & Burton 1984). It is possible to follow these two components along the eastern arm regions until the two arms are separated on the sky, further south-west. If the bulk of the stars that we see were in the nearer arm, then we would expect the ratio of A_V to N_H to be shallower than otherwise expected. This is as expected since the stars from the front arm should be more likely to be detected because of the higher extinction to the rear arm: stars in the rear arm would typically have extinctions ~1 mag larger than in the front arm. In fact, the presence of a small number of regions with high values for A_V/N_H (Fig. 4) suggests that a small fraction of the observed stars are in fact in the rear arm.

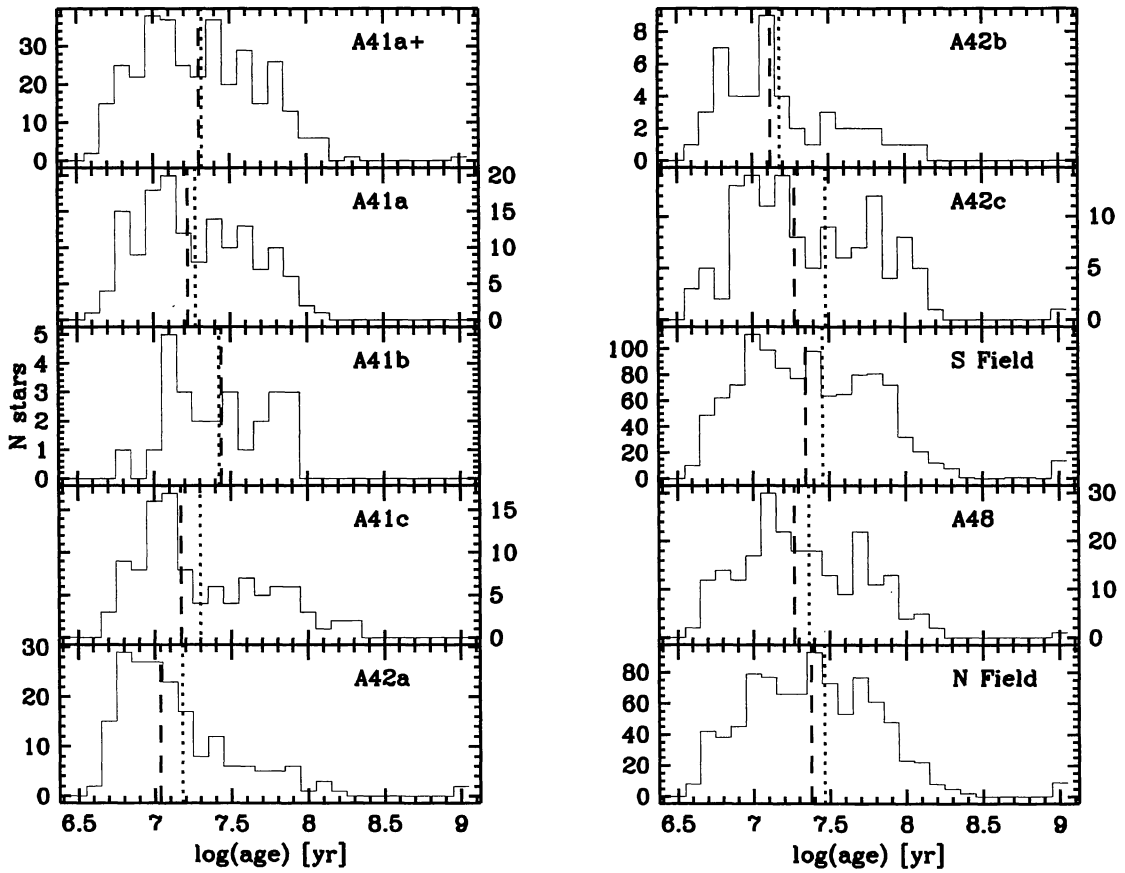

Figure 7. Age distributions determined for each association. We plot the measured ages for the stars in each association as well as all non-association stars for the northern and southern fields. In each figure, the dashed line shows the median value and the dotted line shows the mean value.

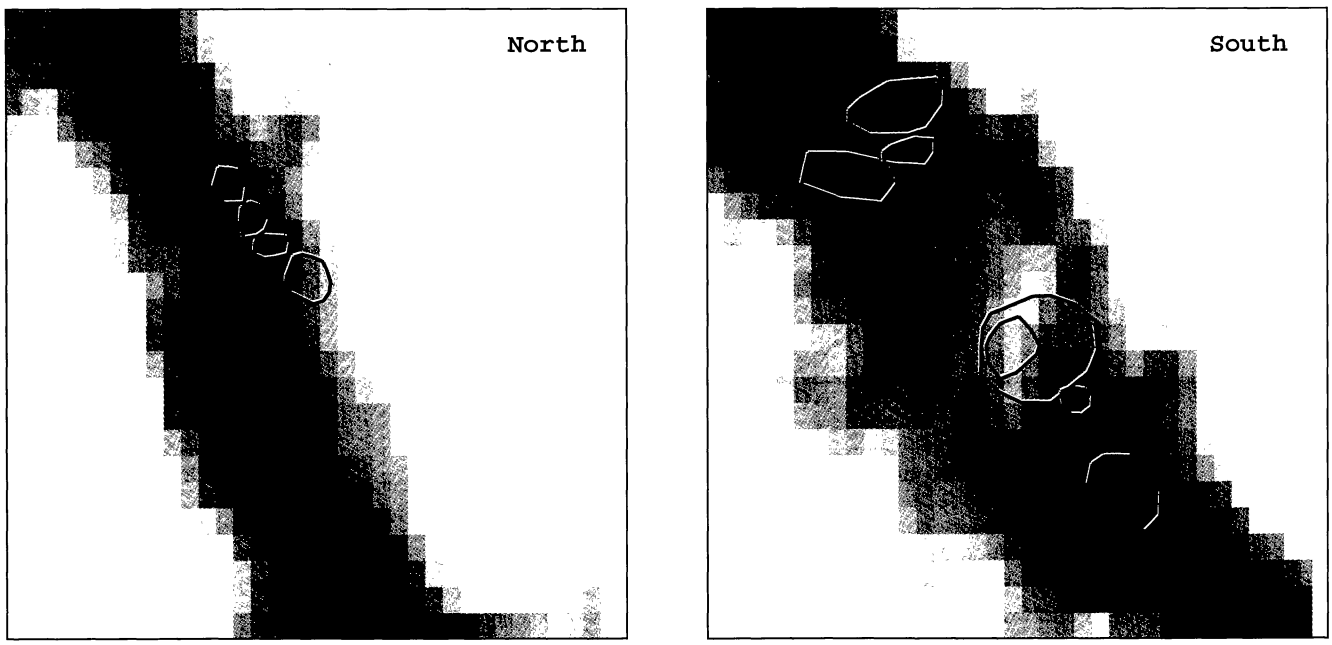

Figure 8. The H I distribution (Brinks & Shane 1984) in the vicinity of our fields. The outlines of the Efremov et al. (1987) associations are also given for comparison. Association A41a is clearly at a local minimum in the H I emission. (See Fig. 1 for identification.)

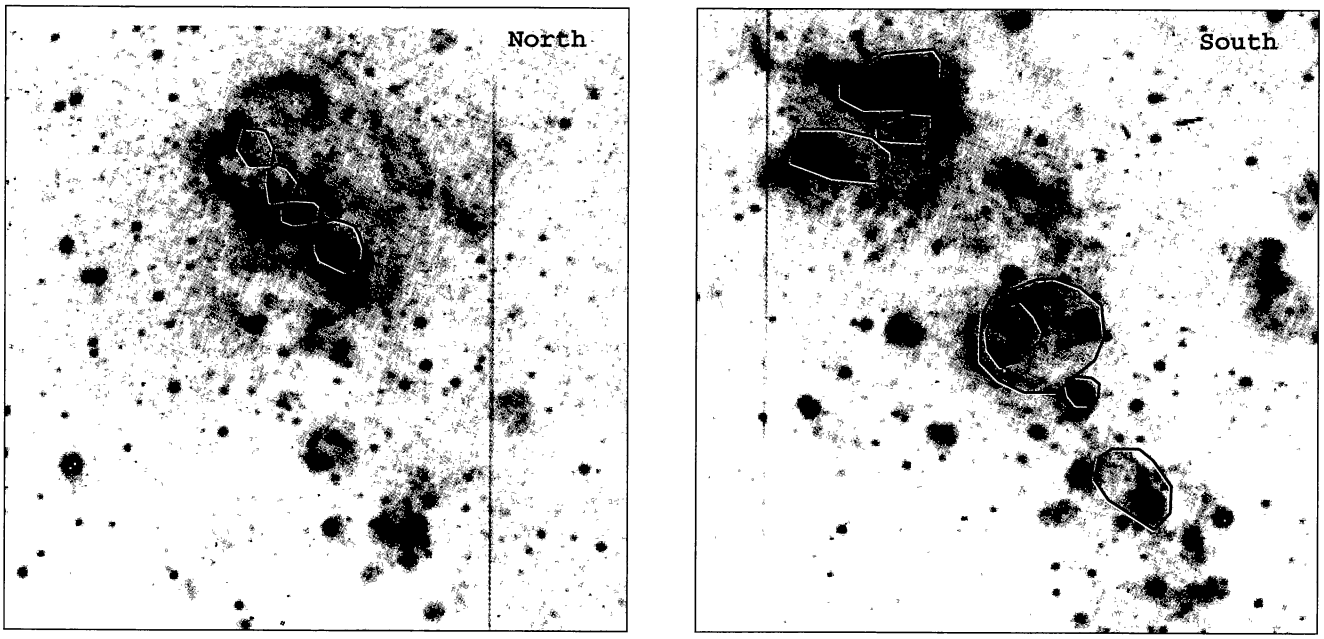

Figure 9. Hα morphology: the grey-scale images are taken in Hα (Magnier et al. 1995). The outlines of the Efremov et al. (1987) associations are also given for comparison. (See Fig. 1 for identification.)

Now that we have determined a probable extinction for each star, we can calculate the unreddened colours. In Figs 5 and 6 we plot CMDs in V, $U-V$ for each of the associations as well as the field stars. We show the raw CMD with the Bertelli et al. (1994) isochrones adjusted for a single, average extinction value for a given group (left-hand side), as well as the extinction-corrected CMD, which suffers from increased errors from the uncertain extinction measurements. We have grouped together the stars from the four A48 associations because of the small number of stars.

The analysis described above to determine the extinction can be used to determine the stellar ages as well. We have taken a weighted average of the logarithmic ages for the five best model fits to each star to determine roughly the stellar age. To test the accuracy of this measurement, we have used the simulations described above. We find that with errors of 0.1 in each filter, we are able to determine the age of a group of stars to ~0.2 in log(age). Because of the photometric cut-off around $V \approx 22.5$ mag, we are only able to determine ages $\lesssim 10^8$ yr.

4 AGE DETERMINATIONS

In Fig. 7, we show the age distribution for each of the Efremov et al. (1987) associations, as well as the stars outside the associations, in the northern and southern regions (N Field and S Field). On each plot, we include a dashed line to represent the median age and a dotted line to represent the mean age of the stars in the sample. In our simulations, both of these measurements tended to overestimate the true age, with the mode of the distribution actually doing a better job in general of determining the input age.

Among the field stars, there is apparently a wide range of stellar ages, with a nearly uniform age distribution. It is important to note, however, that we use the term 'field stars' loosely here: although these stars are not obviously grouped with many other stars, they are clearly not uniformly distributed. It is likely that in many cases we are seeing only the brightest stars of small stellar associations – these are not necessarily individual, isolated stars. The age distribution and surface density of these 'field stars' are similar in the two areas.

Even within the associations, there appears to be a wide range of ages, and a range of coherency for the star formation in different associations. There is a noticeable contrast between associations A41a and A42a, the two largest associations in our field. A42a appears to contain mainly very young stars, with a fairly small range of ages. On the other hand, A41a shows a significant range of ages, and substantially fewer young stars. The median age of A42a is the lowest of the associations in our field at ~10 Myr, while the median age of A41a is among the highest, at ~26 Myr. The distribution of stellar ages for A42a suggests a significant population of very young stars, with ages ~5–10 Myr.

The differences between these two associations are reinforced by the observed morphology of the H I and in these two areas. In Figs 8 and 9 we present maps of the H I and Hα emission in the vicinity of our fields. For the case of A41a, which appears to be relatively old, there is a clear minimum in the H I in this region (Fig. 8) and the Hα emission consists of intricate arc and ring structures (Fig. 9). This suggests that we are seeing the effect of the massive stellar winds on the interstellar medium (ISM) – the general lack of H I emission is what we expect for the H I hole associated with an evolved OB association and the Hα arcs are suggestive of small wind-blown bubbles and supernova remnants from massive stars. This region was in fact noted by Brinks & Bajaja (1986) in their survey as an H I hole (their number 87). For A42a, the H I is a local maximum, and the Hα consists of a large, smooth region of high surface brightness emission, suggesting that the effects of stellar winds have not yet had any significant impact on the ISM in this region. The presence of the Hα emission demonstrates the presence of hot, massive stars.

The association A48 appears to have had an extended period of star formation. The age distribution is quite flat, with a large number of young stars (12 have ages of ~5 Myr), but many intermediate and old (~100 Myr) stars as well. The presence of young stars in this general region has been noted previously. Massey et al. (1986) and

Armandroff & Massey (1991) have identified ~8 Wolf–Rayet (WR) stars within our boundaries of A48. Massey et al. (1995) have identified 10 O and early B stars within the van den Bergh (1964) boundaries of A48 (described as the A48 complex by Efremov et al. 1987). Although most of these luminous blue stars are well outside our boundaries of A48 or consist of blended groups of stars, one star, A48-444, is within our association, and has been classified as an O8I supergiant on the basis of *HST* Faint Object Spectrograph observations (Bianchi, Hutchings & Massey 1996). The presence of this luminous star as well as WR stars implies that star formation has occurred within A48 within the last few Myr. The Hα morphology reflects the range of ages: there are very large arcs/loops, suggesting winds or supernovae from older stars, as well as bright knots of emission as seen for younger stars.

5 CONCLUSIONS

We have observed a series of OB associations in the eastern spiral arm regions of M31 with the WFPC-2 on the *HST* to study the stellar populations. We have used the model evolutionary tracks of Bertelli et al. (1994) to determine stellar parameters.

We have made extinction determinations using a technique which is somewhat different from the standard method of using the locus of stars in a colour–colour plane. Our method makes use of the known distance to allow us to fit the spectral energy distribution in the observed band-passes to Bertelli et al. (1994) models plus extinction. The resulting extinction determinations are shown to be somewhat more accurate than those determined using the colour–colour technique, and allow for a more realistic CMD. Our technique is also better suited to stellar associations with a wide range of extinctions as it is able to determine the best-fitting extinction for each star. This is crucial in these associations in M31, where the extinction is seen to vary over a wide range, up to 2 mag in A_V.

We present comparisons between our optically measured extinction and the observed distribution of H I emission. Although there is a general agreement between the locations of high extinction and high H I column density, the ratio of A_V to N_H is lower than expected. We attribute this to the overlapping of two spiral arms in this region, which is observed in the H I velocity maps (Brinks & Burton 1984).

We are able to determine the age of the stellar groups with an accuracy of ~0.2 in log(age). With this level of accuracy, we are able to detect age differences between several of the richer associations in our fields. The relative ages of these associations agree well with the other indicators of the age available to us: the morphology of the Hα and the morphology of the H I gas.

ACKNOWLEDGMENTS

We acknowledge the support of NASA grant GC-5911-01-94A during the course of this work. We gratefully thank Eli Brinks for FITS versions of the H I maps. We thank the referee for important suggestions.

REFERENCES

Armandroff T. E., Massey P., 1991, AJ, 102, 927
Baade W., 1944, ApJ, 100, 137
Battinelli P., Efremov Yu. N., Magnier E. A., 1996, A&A, 314, 51
Bertelli G., Bressan A., Chiosi C., Fagotto F., Nasi E., 1994, A&AS, 106, 275
Bertola F., Bressan A., Burstein D., Buson L. M., Chiosi C., Di Serego Alighieri S., 1995, ApJ, 438, 680
Bianchi L., Hutchings J. B., Massey P., 1996, AJ, 111, 2303
Brinks E., Bajaja E., 1986, A&A, 169, 14
Brinks E., Burton W. B., 1984, A&A, 141, 195
Brinks E., Shane W. W., 1984, A&AS, 55, 179
Burstein D., Heiles C., 1984, ApJS, 54, 33
Cardelli J. A., Clayton G. C., Mathis J. S., 1989, ApJ, 345, 245
Efremov Yu. N., Ivanov G. R., Nikolov N. S., 1987, Ap&SS, 135, 119
Freedman W., 1989, AJ, 98, 1285
Haiman Z. et al., 1994a, A&A, 286, 725
Haiman Z. et al., 1994b, A&A, 290, 371
Hodge P. W., Lee M. G., 1988, ApJ, 329, 651
Hodge P. W., Lee M. G., Mateo M., 1988, ApJ, 324, 172
Holtzman J. A., Burrows C. J., Casertano S., Hester J. J., Trauger J. T., Watson A. M., Worthey G., 1995, PASP, 107, 1065
Hubble E. P., 1929, ApJ, 69, 99
Humphreys R. M., 1979, ApJ, 234, 854
Magnier E. A., Lewin W. H. G., van Paradijs J., Hasinger G., Jain A., Pietsch W., Trümper J., 1992, A&AS, 96, 379
Magnier E. A., Prins S., van Paradijs J., Lewin W. H. G., Supper R., Hasinger G., Pietsch W., Trümper J., 1995, A&AS, 114, 215
Massey P., Armandroff T. E., Conti P. S., 1986, AJ, 92, 1303
Massey P., Armandroff T. E., Pyke R., Patel K., Wilson C. D., 1995, AJ, 110, 2715
Richer H. B., Crabtree D. R., 1985, ApJ, 298, L13
van den Bergh S., 1964, ApJS, 9, 65
Walterbos R. A. M., Schwering P. B. W., 1987, A&A, 180, 27
Welch D. L., McAlary C. W., McLaren R. A., Madore B. F., 1986, ApJ, 305, 583
Whitmore B., 1995, in Koratkar A., Leitherer C., eds, Calibrating Hubble Space Telescope: Post Servicing Mission. STScI, Baltimore, p. 269
Zombeck M. V., 1990, Handbook of space astronomy and astrophysics. Cambridge Univ. Press, Cambridge

This paper has been typeset from a TEX/LATEX file prepared by the author.